

COM - Compton Scattering

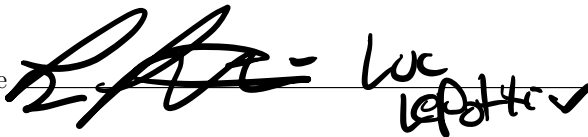
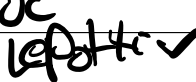
Signature Sheet

Student's Name Rachel Wang Partner's Name Ian Haines

Pre-Lab Discussion Questions

It is your responsibility to discuss this lab with an instructor before your first day of your scheduled lab period. This signed sheet must be included as the first page of your report. Without it you will lose grade points. You should be prepared to discuss at least the following before you come to lab:

1. What is Compton scattering? How does the Compton formula relate to a laboratory experiment?
2. To get an idea of the maximum Compton energy shift for the 59.54 keV photons from the ^{241}Am source, calculate the energy shift for a back-scattered photon off of a free electron.
3. Calculate the energy shift for a back-scattered photon off of an aluminum nucleus. How does this compare to the shift from scattering off of an electron?
4. What is a scattering cross-section? How does the Klein-Nishina formula relate to a laboratory experiment?
5. Use the (classical) Thomson total cross section for scattering to estimate the probability of scattering off of a nucleus compared to the probability of scattering off of an electron. [See Melissinos for information on the Thomson cross-section and cross sections in general.]
6. By what means does the CdTe detector detect photons? (Photoelectric effect? Compton scattering? Pair production? Bremsstrahlung?)

Staff Signature  Luc  Date 9/2/21

Completed before the first day of lab? (Circle one) Yes / No

Mid-Lab Discussion Questions

1. On day 5 of this lab, you should have produced a plot of scattered peak energies versus scattering angle, and made an estimate of the electron mass. Show them to a GSI and ask for a signature.

Staff Signature  Date _____


Completed by day 5 of lab? (Circle one) Yes / No

Checkpoint Signatures

1. Optimal Energy Range

Staff Signature _____

2. Apparatus Safety

Staff Signature _____

3. Data Collection

Staff Signature _____

4. Radiation Flux

Staff Signature _____

5. Over-the-Weekend Measurement

Staff Signature _____

Compton Scattering: The Compton Effect and Klein-Nishina Corrections

Ian Haines*

*Department of Physics, University of California,
Berkeley, 366 Physics North, Berkeley, CA 94720*

(Dated: September 28, 2021)

The Compton effect has its history in overturning the classical understanding of light scattering via free electrons. Compton's work proved to be important for the formulation and experimental validation of quantum mechanics. The Compton effect was observed for a ^{241}Am source and ^{13}Al targets with varying radii for 5 angles with a pulse-height analyzer. Results showed $\chi^2 = 0.0109$ for the Compton scattering hypothesis. The Compton Hypothesis was accepted. This acceptance showed the mass of the electron to be $m_e = 520 \pm 21$ keV. The Klein-Nishina hypothesis predicted the correct order of magnitude for electron scattering energies. Analysis and discussion of results is included.

Keywords: Compton scattering, Klein-Nishina, quantum mechanics, quantum electrodynamics, nuclear physics, atomic physics

I. INTRODUCTION

During the late 19th and early 20th century, it had been believed that light-matter interactions were governed by classical electrodynamics. Specifically, the Thomson differential scattering cross section predicted preferential scattering at 90 degrees and a symmetric scattering angle distribution about 90 degrees. Furthermore, the Thomson formula is energy invariant and so predicted the same results for high or low intensity beams of light. Compton's experiment showed the insufficiency of the Thomson differential scattering cross section to explain the phenomena he observed. Not only did Compton show that the scattering angular distribution predicted by the Thomson formula is wrong but also that light behaves like a particle in the interaction imparting some energy onto the electron as it elastically scatters [1].

Merely five years after Compton's experiment, Klein and Nishina investigated the Compton effect using the then recently derived Dirac equation. Klein and Nishina showed that the predictions of Compton and quantum mechanics were still insufficient to explain the distribution of the scattering angle of sufficiently high energy photons. Klein and Nishina's formula predicted that the scattering angle distribution skewed towards small angles as the energy increased [2].

A. Compton's Picture

Compton's picture can be described as follows: suppose the frame of reference is the lab-frame and a photon, γ , moves with momentum \mathbf{p} striking a free electron e^- with zero momentum. After the collision, γ will scatter at an angle θ and have momentum \mathbf{p}' while e^- will scatter at an angle ψ and have momentum \mathbf{q}' (See Fig.

1). It can be shown using conservation of 4-momentum [3] that

$$\lambda' - \lambda = \frac{h}{m_e c^2} (1 - \cos \theta) \quad (1)$$

where λ is the initial wavelength and λ' is the wavelength after scattering. The more useful, but mathematically equivalent, formula for a pulse-height analyzer apparatus is given as

$$E_{\gamma'} = \frac{E_{\gamma}}{1 + \left(\frac{E_{\gamma}}{m_e c^2}\right)(1 - \cos \theta)} \quad (2)$$

where E_{γ} is the energy of γ before scattering, $E_{\gamma'}$ is the energy after scattering, and m_e is the mass of e^- . An important limit is the low energy limit where $E_{\gamma} \ll m_e c^2$. In this limit, the relationship shows $E_{\gamma'} \approx E_{\gamma}$ and there is no observed Compton effect. So, high energy photons should be used to observe the effect in practice. Another important implication of this equation is that it predicts $E_{\gamma'}$ to decrease as θ increases with $E_{\gamma'}$ reaching a minimal value at $\theta = \pi$. Thus, energy differences should correspond with angle. One final observation is that $E_{\gamma'}/E_{\gamma} \propto 1 + m^{-1}$ so that if the incident photon strikes the nucleus of the atom instead of a free electron, then the observed energy shift will be roughly 0. This explains the observed phenomenon where it appears photons retain their energy despite scattering.

* ianphaines@berkeley.edu

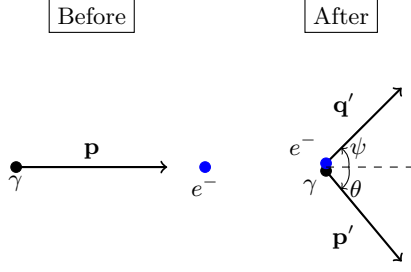


FIG. 1. Compton scattering picture in laboratory frame. On the left side of the figure is γ moving with momentum \mathbf{p} towards e^- before the scattering. On the right side of the figure is γ moving with momentum \mathbf{p}' and e^- moving with momentum \mathbf{q}' . Two important notes are (i) $\theta \neq \psi$ and (ii) the depiction doesn't show the wavelength/frequency shift of γ after scattering.

B. Klein and Nishina's Corrections

Starting from Compton's picture, it can be shown using perturbation theory in quantum electrodynamics [4] that

$$\frac{d\sigma}{d\Omega} = \frac{1}{2}\alpha^2 r_c^2 P(E_\gamma, \theta)^2 \left[P(E_\gamma, \theta) + P(E_\gamma, \theta)^{-1} - \sin^2 \theta \right] \quad (3)$$

where α is the fine-structure constant, $r_c = \frac{\hbar}{m_e c^2}$ is the reduced Compton wavelength, and $P(E_\gamma, \theta)$ is the fractional change in energy or (2) divided by a factor of E_γ . This is the celebrated differential scattering cross-section given by Klein and Nishina. Important to note is the low energy limit where $P(E_\gamma, \theta) \rightarrow 1$. In this limit, using some Pythagorean identities yields the Thomson differential scattering cross-section. Also important to note is that this function is asymmetric about $\frac{\pi}{2}$ with increasing asymmetry as E_γ increases until forward scattering is almost entirely favored (See Figures 2 and 3). Using the chain rule and azimuthal symmetry, it is possible to show (see Appendix A) that

$$\frac{d\sigma}{dq'} = \frac{d\sigma}{d\Omega} \frac{2\pi m_e c^2}{k'^2} \quad (4)$$

where q' is the energy of the electron after scattering and k' is the energy of the photon after scattering (see Fig. 4).

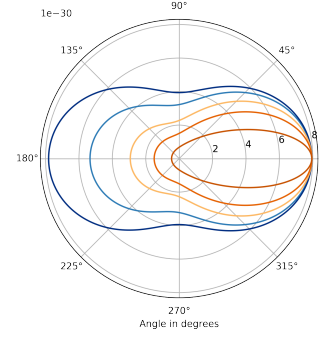


FIG. 2. Klein-Nishina distribution for energies 2 keV, 59.54 keV, 200 keV, 500 keV, and 2 MeV. Increasing color warmth corresponds to increasing energy of the incoming photon. Apparent from the plot is the symmetry in scattered angle for 2 keV but extreme asymmetry in scattered angle for higher energies and increasing asymmetry as energy increases.

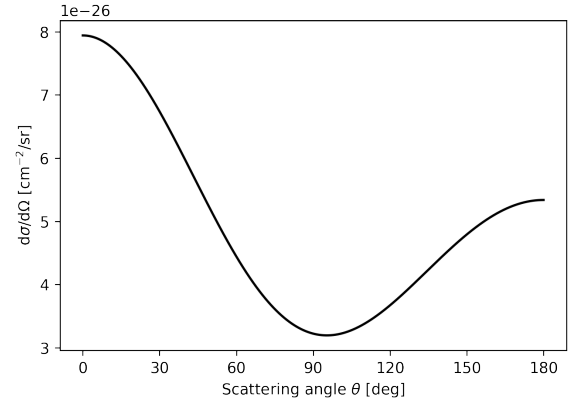


FIG. 3. The probability of finding a photon at 90 degrees decreases by roughly a factor of 2 relative to finding a photon at 30 degrees. In principle, it should be expected that forward scattering is more likely to occur.

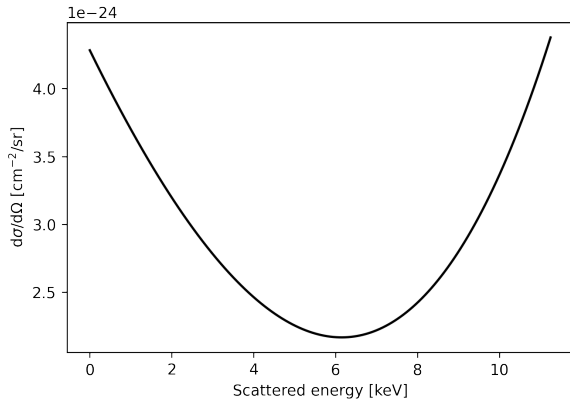


FIG. 4. The distribution of scattered electron energies from an incident 59.54 keV photon. Due to the asymmetry in the scattering angle, an asymmetry in the scattered electron energy manifests.

II. EXPERIMENTAL DESIGN AND APPARATUS

^{241}Am was used as a source of hard X-rays. Hard X-rays are ideal because they have smaller wavelengths and thus higher energies. The most frequently emitted X-ray from ^{241}Am has an energy of 59.54 keV. ^{241}Am emits X-rays of lesser energies too, but these energies are less than half the energy of the primary energy beam (see Fig. 5) and so they do not interfere with the detection of scattered photons. In conjunction with the ^{241}Am source was a ^{13}Al target. This target was used because ^{13}Al has a $3p^1$ valence electron which behaves as a free electron. This makes ^{13}Al an ideal target for observing the Compton effect.

In this experiment, the source sat atop a fixed block while the target rod stood roughly 7 cm away from the source. The CdTe detector and pulse-height analyzer (PHA) combination rested on a swivel roughly 7 cm away from the target. The detector-PHA unit was then rotated to different angles created by the source, target, and detector (See Fig. 6). This allowed for capture of scattered X-rays at different angles.

A. CdTe Detector and Pulse-Height Analyzer

A CdTe detector and pulse-height analyzer were used to detect the scattered X-rays and determine their energies. The CdTe detector consists of an intrinsic semiconductor connected to an amplifier. When a photon strikes the semiconductor, the energy is transmitted into electron-hole pairs which move in opposite directions. This creates a current through the circuit which is then amplified and sent to the pulse-height analyzer. The pulse-height analyzer then digitizes the signal and analyzes the height of it to determine the energy and puts

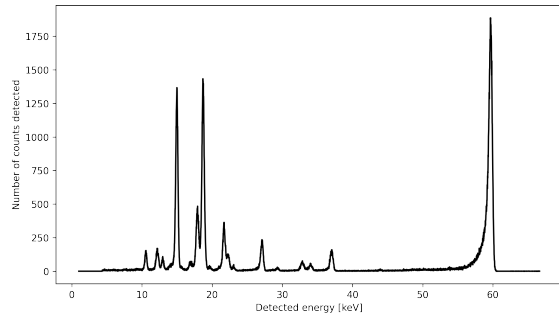


FIG. 5. Raw ^{241}Am spectrum obtained using the XR-123 CdTe detector. Of important note is the peak to the right and its asymmetry. This peak corresponds to the 59.54 keV X-ray which is the desired source of incident photons.

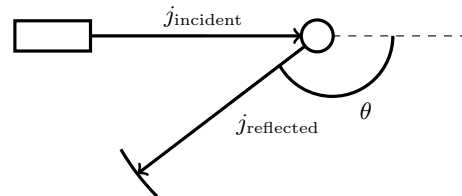


FIG. 6. Depiction of the working experiment. The source emits an incident flux of X-rays onto the target which then scatter at different angles. The detector is fixed at an angle θ which receives a reflected flux. This received flux is then analyzed by the PHA and sent to the computer for binning.

it into a corresponding bin of a histogram. After this process, the data is sent to a computer terminal on which a program is used to collect the data and format it neatly to be used for analysis.

A question must be asked: what is the resolution of the detector? The importance of this question lies in the fact that the resolution determines the finite accuracy achievable and therefore the uncertainty in the determination of the energy spectrum in a scattering experiment. The resolutions (FWHM of peak divided by peak height) of the XR-123 CdTe detector are given below in Table 1. These resolutions correspond to how inaccurate the detector is at determining which bin a photon should be placed in. The lower the resolution percentage, the greater the accuracy in determining which photon should go in which bin.

TABLE I. Full-width at half-maximum and resolution for each peak in the ^{241}Am spectrum. The FWHM are on the order of 1 part in 1000 times the size of the peaks which result in the resolution percentage numbers seen.

E_γ [keV]	FWHM [eV]	R
13.5	374 ± 16	$(2.74 \pm 0.12) \times 10^{-2} \%$
17.3	274 ± 16	$(2.61 \pm 0.11) \times 10^{-2} \%$
20.9	423 ± 16	$0.116 \pm 0.044 \%$
26.3	488 ± 16	$0.208 \pm 0.069 \%$
59.54	602 ± 16	$(3.19 \pm 0.08) \times 10^{-2} \%$

B. Calibration

The detector had been calibrated before data collection. This is important as the PHA is a multi-channel analyzer and so the data seen on the screen corresponds to bin numbers and not energies. A conversion must be made between bin or channel number and the energy of the corresponding bin. Runs were performed with 4096 channels. The highest peak of the raw spectrum corresponded to 59.54 keV photons (see Fig. 5). Thus, it is easy to find the conversion between bin number and photon energy by dividing 59.54 by the bin number corresponding to it. Each bin had a corresponding width of 0.01627 keV. It is essential that the detector be setup so that photons below a certain energy threshold are ignored. Important for data analysis is time normalization. Each count adds time to the live detection time, so noise from low energy photons being detected obscures the true live detection time.

III. RESULTS AND ANALYSIS

A. Collected Data and Data Munging

Scattering and background data was captured for 5 angles: 30, 60, 80, 100, and 145 degrees. Appendix B gives further representations of the data. Different rods were used to capture data for different angles (see Table 2).

In the data collection process, there is background which accumulates from the X-rays that pass through or scatter off of objects without scattering off of the target itself. These photons accumulate for angles $\theta \leq 100$. It is important in the determination of the true peak energy and energy uncertainty to normalize by subtracting this background value from the collected data. To do this, requires a time normalization process in which the total number of counts for a bin is divided by the live time (time that the detector is actually registering scattered photons) which gives the yield for that bin (see Table 3). The background data bin values can then be subtracted from the actual data bin values.

TABLE II. Different radius rods were used corresponding to the angle. For angles with smaller cross-sections, larger radius rods tended to be used to increase the probability of scattering so as to obtain usable data.

Angle [deg]	Rod Radius [cm]
30	0.635
60	0.952
80	1.90
100	2.54
145	2.54

TABLE III. Time of collection for each angle. Note that t_{bg} is time of background data collection and $t_{scat.}$ is the time of the scattering data collection.

Angle [deg]	$t_{scat.}$ [s]	t_{bg} [s]
30	6637	1563
60	4460	22405
80	11190	62.50
100	72120	83734
145	4748	

The peaks of the scattering data were determined by finding the mean photon energy of photons residing within a certain window around the peak of the distribution. The uncertainty in this peak was determined by calculating the standard deviation of the photons residing within the window (see Table 4). Data had to be rebinned after the background subtraction to smooth out the sharp discontinuities from bin to bin. This gives rise to obvious distributions (see Appendix B).

TABLE IV. Energies of shifted peak after scattering and the uncertainty of this peak energy.

Angle [deg]	Peak Energy [keV]	Peak Uncertainty [keV]
30	57.4	1.0
60	55.6	1.0
80	54.3	1.2
100	52.6	0.4
145	48.8	1.4

B. Compton's Hypothesis

The Compton hypothesis was tested using these values (see Fig. 9). The data clearly shows a linear relationship between the peak energy and the energy predicted by (2) for the given angle. Additionally, each data point with its uncertainty crosses the one-to-one line giving greater certainty that the Compton hypothesis does fit the observed data. The data appears to be randomly distributed about the one-to-one line which indicates that there is no systematic error in the experiment. Therefore, a χ^2 analysis will produce meaningful results. Calculations revealed

$\chi^2 = 0.0109$ and $\chi^2/\text{d.f} = 2.72 \times 10^{-3}$ which indicates that the Compton hypothesis cannot be rejected.

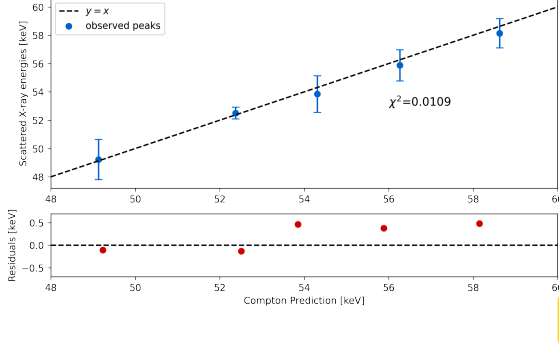


FIG. 7. Comparison between Compton predictions for each angle and an initial incident energy of 59.54 keV and the observed scattering energies.

Important to note is that there are several geometric effects which might affect the distribution of the scattering energies:

1. The beam emitted from the source has a spread in the momentum transverse to the direction of incidence in 2-dimensions. This has the effect of causing the beam to scatter from points that aren't at the center of the target. The effect of this is that there is an induced spread in the angle in both a vertical and horizontal direction.
2. The measured beam angle changes depending on where the beam scatters from inside the target. If the detector makes an angle with the source that is greater than 90 degrees, the front end scattering will be smaller than the nominal value and back end scattering will be larger than the nominal value. Similarly, the situation is opposite if the angle between the source and detector is less than 90 degrees.

These both create a spread in the measured angle, σ_θ . Varying θ in (2) gives

$$\sigma_E = E'_\gamma \frac{\sin \theta}{m_e c^2} \sigma_\theta \quad (5)$$

So this spread in the angle creates a spread in the distribution itself and doesn't actually shift the peak. It is important to note, however, that the spread in peak energy depends upon the post-scattering energy and the angle of scattering so that it is not invariant with respect to either of these quantities.

Another possible source of error is in the live time measurement by the detector. For the 60 and 145 degree runs, the detector rejection threshold had been set to be too low. As a result, ambient light scattering inside of the detector had been adding time to the live time. No numerical calculation could be used to undo the effects

of this procedural error. This error created a large uncertainty in the live times of both the 60 and 145 degree runs. The result of this error can be understood as follows:

$$n_{true} = n_{data} - n_{bg} \quad (6)$$

where n_{data} is the time-normalized value at each bin and n_{bg} is the time-normalized value at each bin. Now, $n = N/t$ where N is the nominal value of the bin and t is the live-time. This causes an uncertainty:

$$\sigma_{n_{true}} = \sqrt{\frac{N_{data}}{t_{data}^2} \sigma_{t_{data}}^2 + \frac{N_{bg}}{t_{bg}^2} \sigma_{t_{bg}}^2} \quad (7)$$

The uncertainty chosen in this analysis was the width of the distribution because it captures both of the uncertainties described above.

Assuming that the Compton hypothesis is correct, the mass of the electron can be measured. Now, m_e is treated as an unknown parameter to be found by minimizing the χ^2 value by varying m_e . This turns (2) into a family of distributions:

$$E_{\gamma'}(E_\gamma, \theta; m_e) = \frac{E_\gamma}{1 + \left(\frac{E_\gamma}{m_e c^2}\right)(1 - \cos \theta)} \quad (8)$$

where m_e is the sole parameter characterizing the distribution. By performing a non-linear fit to the data obtained previously, it is possible to find the mass of the electron that best fits the data (see Table 5).

TABLE V. Energies of shifted peak after scattering and the uncertainty of this peak energy.

Actual m_e [MeV]	Fit m_e [MeV]	Relative Error
0.510	0.520 ± 0.011	1.90%

C. Klein-Nishina Hypothesis

In the final section of this experiment, a beam emitted from the source was collimated by a brass plate and lead sheet unit with a 1mm wide aperture which screened for low energy photons so that only 59.54 energy photons entered the detector. These photons underwent Compton scattering with the electrons in the detector-PHA unit (see Fig 8).

The differential scattering cross-section takes on the intuitive form [5]:

$$\frac{d\sigma}{d\Omega} = \frac{\text{yield}}{d\Omega N I_0} \quad (9)$$

where the yield is the number of 59.54 keV photons divided by the efficiency of the detector for that energy level [6], N is the number of electrons of the detector, and I_0 is the photon flux at the source.

The number of electrons was determined using the following formula

$$N = A_{\text{det.}} \rho_{\text{CdTe}} \frac{N_A}{A_{\text{CdTe}}} Z_{\text{CdTe}} \quad (10)$$

where $A_{\text{det.}} = 3\text{cm} \times 3\text{cm}$ is the area of the detector, ρ_{CdTe} is the density of CdTe, N_A is Avogadro's number, A_{CdTe} is the weighted atomic mass of CdTe, and Z_{CdTe} is the weighted atomic number of CdTe where the weights are given by the percentages of each element within the crystal.

The photon flux at the source, I_0 , can be determined by integrating over the entire spectrum and dividing by the live time. Additionally, $I \propto r^{-2}$ and so a factor of the distance between the source and detector squared must be included.

These calculations yielded the final result in Figure 9. The order of magnitude of the observed spectrum matches the predicted order of magnitude; however, there are large inconsistencies between the theoretical predictions and the observed data. Moreover, the trend in the data does not match the trend in the prediction. At the higher scattered electron energies, the observed distribution is flat; whereas, the theory predicts an increasing slope with increasing energy.

Some possible explanations for this deviation from observed and expected are systematic. In this model, it is assumed that the photons only interact once with the electrons within the CdTe crystal. If a photon were to interact twice, that would possible cause the increased number in low energy scattered electrons. Additionally, this model does not take into account electron-electron interactions which could also cause some energy to not be accounted for; again, this would cause the low energy scattered electron count to increase while the high energy electron count would decrease.

It can be said with certainty that $d\Omega$, N , and I_0 are all constant for this run. The only random variable in this case is the yield, and so it is the uncertainty in this that leads to the deviation from theory, assuming that the theory is robust and should be accepted. While the Klein-Nishina hypothesis cannot be confirmed, the fact that it does predict the correct order of magnitude means that it would be unwise to outright reject it.

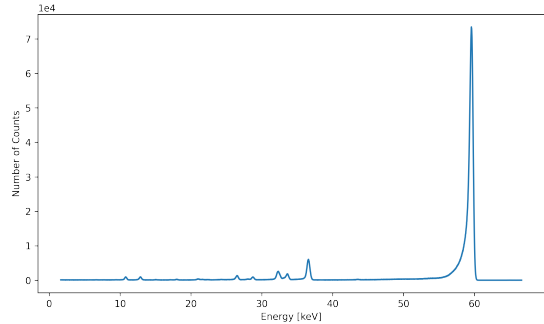


FIG. 8. Spectrum collected to verify the Klein-Nishina hypothesis. Not pictured is the large tail at the low-energy regime composed of ambient light photons.

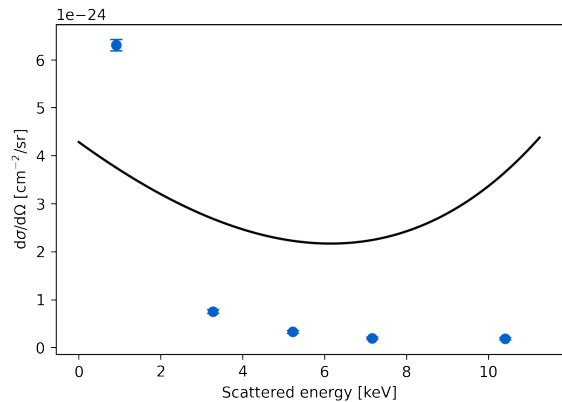


FIG. 9. Observed scattered electron energy distribution. The order of magnitude matches with the prediction, but the actual values themselves have large errors.

IV. CONCLUSION

The Compton effect and Compton scattering are staples in the young physicist's education and serve to introduce them to the world of quantum mechanics and how experiments can validate the predictions of quantum mechanics. In this experiment performed, the Compton hypothesis was affirmed. By assuming that the Compton hypothesis was correct, the mass of the electron was then deduced by considering it as a parameter to be chosen to maximize the likelihood of the data matching the prediction. There are systematic errors in this procedure that must be accounted for when performing a fit of scattering data to the Compton formula. Lastly, while the Klein-Nishina corrections did provide the correct order of magnitude for the observed data, there are systematic errors that have not been accounted for and further exploration is warranted to determine more accurately the goodness-of-fit of the hypothesis to the data.

ACKNOWLEDGMENTS

I wish to acknowledge Rachel Wang for her work in performing this experiment with me and analyzing the data, Professors Holzapfel and Stamper-Kurn for their guidance and support in answering questions, GSI Luc Le Pottier for his guidance and support in performing the experiment, and Winthrop "The Wizard" Williams for maintaining the laboratory and assembling the apparatus used for this experiment.

Appendix A: Distribution of Electron Energies Proof

In the introduction it had been claimed that

$$\frac{d\sigma}{dq'} = \frac{d\sigma}{d\Omega} \frac{2\pi m_e c^2}{p'^2} \quad (\text{A1})$$

It is here that we prove this claim.

The chain rule can be used to rewrite the left-hand side as

$$\frac{d\sigma}{dq'} = \frac{d\sigma}{d\Omega} \frac{d\Omega}{dq'} \quad (\text{A2})$$

or

$$\frac{d\sigma}{dq'} = \frac{d\sigma}{d\Omega} \left(\frac{dq'}{d\Omega} \right)^{-1} \quad (\text{A3})$$

Now, the scattering is azimuthally symmetric so $d\Omega = 2\pi \sin \theta d\theta$ and so

$$\frac{dq'}{d\Omega} = \frac{1}{2\pi \sin \theta} \frac{dq'}{d\theta} \quad (\text{A4})$$

Due to energy conservation

$$p - p' = q' \quad (\text{A5})$$

which can be rewritten using (2)

$$p - p' = p - \frac{p}{1 + \frac{p}{m_e c^2} (1 - \cos \theta)} \quad (\text{A6})$$

Differentiating this with respect to θ gives

$$\frac{dq'}{d\theta} = \frac{p^2}{\left[1 + \frac{p}{m_e c^2} (1 - \cos \theta) \right]^2} \frac{1}{m_e c^2} \sin \theta \quad (\text{A7})$$

Performing some algebra and realizing the first factor is just p' yields

$$\frac{1}{2\pi \sin \theta} \frac{dq'}{d\theta} = \frac{p'}{2\pi m_e c^2} \quad (\text{A8})$$

This completes the proof of the claim.

Appendix B: Tables and Graphs of Results

Below are graphs of a 50 point running average of the background counts which have been time normalized. The reason these have been time normalized is to smooth out the discontinuities in count number as a function of bin number. These discontinuities arise due to the discrete nature of the data collection.

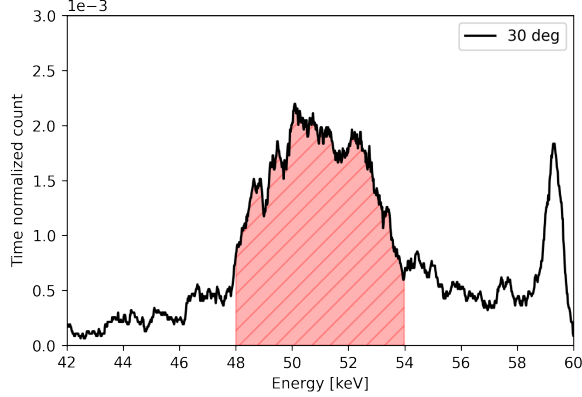


FIG. 10. The time normalized background counts for scattering at 30 degrees. The peak of these counts appears to correspond to roughly ~ 51 keV and the distribution (red hatch-marked area) in the range from 48 – 52 keV is roughly symmetric about this peak.

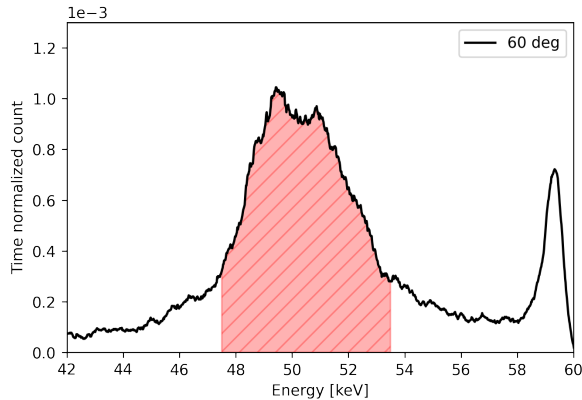


FIG. 11. The time normalized background counts for scattering at 60 degrees. The peak of these counts appears to correspond to roughly ~ 50.5 keV and the distribution (red hatch-marked area) in the range from 47.5 – 51.5 keV is roughly slightly asymmetric about this peak.

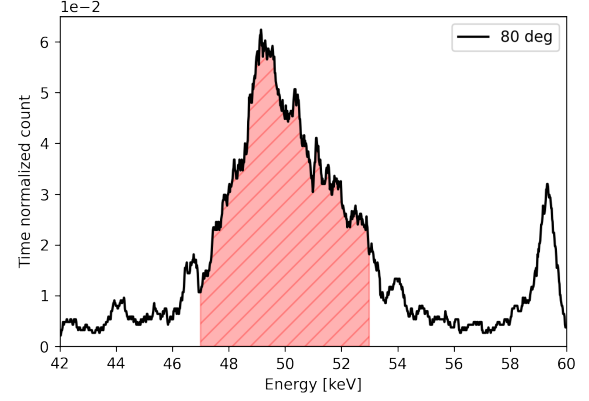


FIG. 12. The time normalized background counts for scattering at 80 degrees. The peak of these counts appears to correspond to roughly ~ 49.5 keV and the distribution (red hatch-marked area) in the range from 47 – 53 keV is slightly asymmetric about this peak.

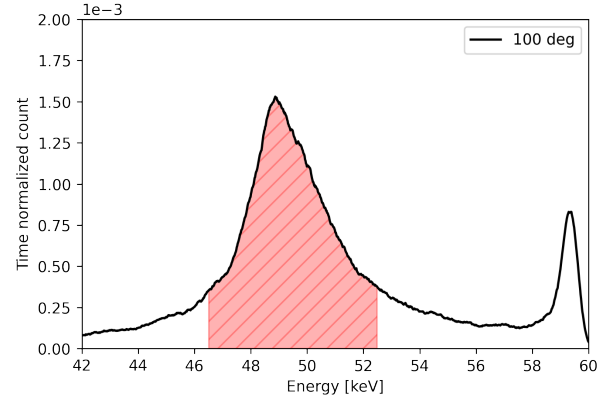


FIG. 13. The time normalized background counts for scattering at 100 degrees. The peak of these counts appears to correspond to roughly ~ 49 keV and the distribution (red hatch-marked area) in the range from 46.5 – 52.5 keV is clearly asymmetric about this peak.

TABLE VI. Background integrated counts (IC) and time normalized integrated counts (TNIC). At peak indicates that only data falling under the red hatched range in the corresponding figures was used in the calculations.

	30 deg	60 deg	80 deg	100 deg
IC	1593	9373	1291	41522
TNIC	0.3844	0.4183	0.2066	0.4958
IC _{peak}	906	5804	830	26202
TNIC _{peak}	0.2186	0.2590	0.1328	0.3129

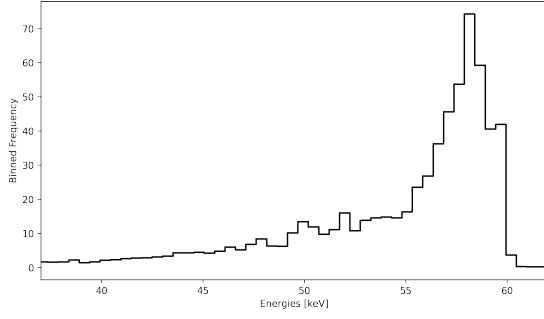


FIG. 14. Rebinned 30 degree scattering data after background subtraction. The data here has been time and volume normalized so as to be comparable to data for other angles

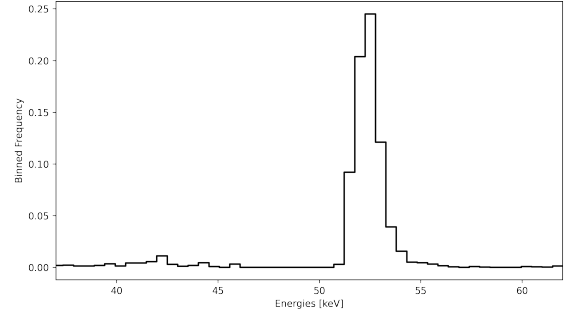


FIG. 17. Rebinned 100 degree scattering data after background subtraction. The data here has been time and volume normalized so as to be comparable to data for other angles.

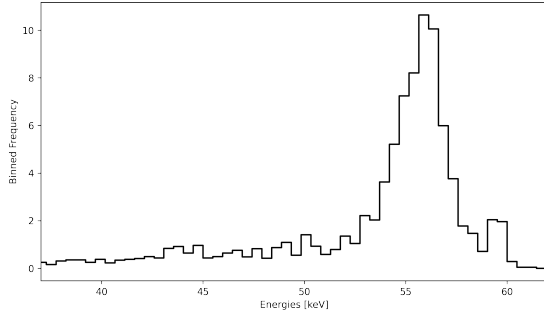


FIG. 15. Rebinned 60 degree scattering data after background subtraction. The data here has been time and volume normalized so as to be comparable to data for other angles.

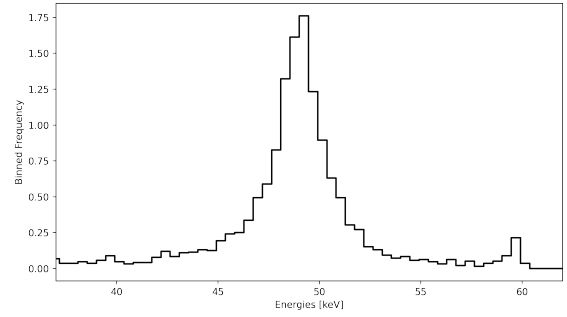


FIG. 18. Rebinned 145 degree scattering data after background subtraction. The data here has been time and volume normalized so as to be comparable to data for other angles.

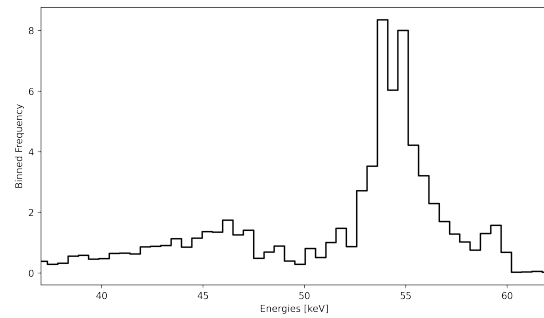


FIG. 16. Rebinned 80 degree scattering data after background subtraction. The data here has been time and volume normalized so as to be comparable to data for other angles.

-
- [1] A. H. Compton, A quantum theory of the scattering of x-rays by light elements, *Phys. Rev.* **21**, 483 (1923).
 - [2] O. Klein and Y. Nishina, *Nature* **122**, 398 (1928).
 - [3] G. Farmer, Derivation of compton scattering relation in covariant notation, *Am. J. Phys.* **34**, 614 (1966).
 - [4] S. Weinberg, *The Quantum Theory of Fields*, Vol. 1 (Cambridge University Press, 1995) Chap. 8, pp. 362–368.
 - [5] A. C. Melissinos and J. Napolitano, *Experiments in modern physics; 2nd ed.* (Academic Press, New York, NY, 2003).
 - [6] R. B., *Efficiency of Amptek XR-100T-CdTe and -CZT Detectors Application Note ANCZT-1 Rev 2.*